From bench to cell: a roadmap for assessing the bioorthogonal “click” reactivity of magnetic nanoparticles for cell surface engineering

Javier Idiago-López,[a,b] Eduardo Moreno-Antolín,[a] Maite Eceiza,[c] Jesús M. Aizpurua,[c] Valeria Grazú[a,b] Jesús M. de la Fuente[a,b] and Raluca M. Fratila*[a,b,d]*

[a] *Instituto de Nanociencia y Materiales de Aragón, INMA (CSIC-Universidad de Zaragoza), C/ Pedro Cerbuna 12, 50009, Zaragoza, Spain.*

[b] *Centro de Investigación Biomédica en Red de Bioingeniería, Biomateriales y Nanomedicina, Instituto de Salud Carlos III, Spain.*

[c] *Universidad del País Vasco, UPV-EHU, Jose Mari Korta R&D Ctr, PO 20018, Donostia San Sebastián, Spain.*

[d] *Departamento de Química Orgánica, Facultad de Ciencias, Universidad de Zaragoza, C/ Pedro Cerbuna 12, 50009, Zaragoza, Spain.*

Corresponding authors: Jesús M. de la Fuente (j.m.fuente@csic.es; jmfuente@unizar.es); Raluca M. Fratila (rfratila@unizar.es)

KEYWORDS: bioorthogonal chemistry, cell membrane, metabolic glycoengineering, magnetic nanoparticles

ABSTRACT. In this work, we report the use of bioorthogonal chemistry, specifically the strain-promoted click azide-alkyne cycloaddition (SPAAC) for the covalent attachment of magnetic nanoparticles (MNPs) on living cell membranes. Four types of MNPs were prepared, functionalized with two different stabilizing/passivation agents (a polyethylene glycol and a glucopyranoside derivative, respectively) and two types of strained alkynes with different reactivities: a cyclooctyne (CO) and a dibenzocyclooctyne (DBCO) derivative. The MNPs were extensively characterized in terms of physico-chemical characteristics, colloidal stability and click reactivity in suspension. Then, the reactivity of the MNPs towards azide-modified surfaces was evaluated, as a closer approach to their final application in a living cell scenario. Finally, the DBCO-modified MNPs, showing superior reactivity in suspension and on surfaces, were selected for cell membrane immobilization via SPAAC reaction on the membranes of cells engineered to express azide artificial reporters. Overall, our work provides useful insights into the appropriate surface engineering of nanoparticles to ensure a high performance in terms of bioorthogonal reactivity for biological applications.

Introduction

Cell membranes are very complex and dynamic systems, which not only act as physical barriers, but also play key roles in the regulation of cellular functions and dictate the way cells interact with their environment. In this regard, cell surface engineering arises as a promising approach for conferring cells new properties and functions and has potential applications in the field of cell therapy,[1,2] biosensing,[3] bioimaging[4] and diagnosis.[5] Traditionally, genetic engineering has been widely used to modify the expression of cell surface proteins with different therapeutical purposes.[6,7] However, the intrinsic limitations of efficient gene transfection and the need to face more complex scenarios where not only surface proteins are involved have motivated the search for new alternatives for cell surface modification, based on the chemical modification of cell membrane biomolecules and material science.[8] Nanomaterials and their singular physicochemical properties have attracted attention for cell surface engineering for the development of new therapeutic and diagnostic applications. Examples of such applications include the immobilization of drug-loaded nanoparticles (NPs) onto immune or stem cells to exploit tissue-homing properties toward hypoxic or necrotic tissues related with cancer,[9,10] the surface labelling of cells with NPs with optical properties for tracking their fate after *in vivo* transplantation[11] or the immobilization of patches carrying magnetic nanoparticles (MNPs) onto lymphocytes for their spatial manipulation with a magnetic field.[12]

The most common approaches described so far for the conjugation of NPs with cells are based on ligand-receptor recognition and on covalent binding. The first one implies the functionalization of the NPs with biomolecules (antibodies, peptides, vitamins, carbohydrates or aptamers)[13] that recognize specific receptors on the cell membrane and bind them through non-covalent bonds. The second approach relies on the formation of covalent bonds between NPs and chemical motifs

available on cell membranes (mainly amine and thiol groups present in membrane proteins[14]). However, both approaches present crucial limitations in terms of efficiency and selectivity. Ligand-receptor interactions are usually of transient nature and can promote a rapid internalization of the NPs,[1,15] which can be problematic if their intended application requires a relatively long retention time on the cell membrane (for instance, for remote control or stimulation of membrane receptors, such as thermo- and mechanosensitive ion channels). On the other hand, the active orientation of the biomolecules once immobilized onto the NPs must be maintained and a high degree of control over the biomolecule display on the NP surface might be necessary in order to ensure that the binding affinity towards the cell receptors is not diminished.[16] In the case of covalent conjugation to naturally occurring chemical groups, the efficiency of the NP immobilization on the cell membrane is dictated by the density and availability of these pre-existing chemical motifs, which furthermore can vary significantly from cell to cell. Moreover, maleimides or activated esters (which are the typical reagents used in the covalent reaction) present low stability in biological media and can randomly conjugate to proteins in the cell culture medium, diminishing the reaction efficiency.[17]

Recently, bioorthogonal ~~chemistry~~ reactions, which can take place inside living systems with complete specificity and minimal interference with native biological processes, have emerged as a powerful alternative for NP-cell coupling.[18,19] One of the most popular to date is the strain-promoted click azide-alkyne cycloaddition (SPAAC).[20] In particular, the synergy between SPAAC chemistry and metabolic glycoengineering has enabled a new strategy for active cell targeting with NPs that overcomes the limitations of the traditional approaches mentioned above, especially related to the heterogeneity of receptors between different types of cells or their limited density.[21] Azide bioorthogonal reporters can be introduced *ad hoc* on cell membrane glycocalyx using the

cell's own metabolic machinery. These artificial chemical receptors can react with NPs functionalized with complementary strained alkyne probes, and to date, this approach has been used to successfully target different types of NPs to cell membranes.[11,19,22]

Despite the great potential that bioorthogonal click chemistry offers for the binding of NPs to cell surfaces, the success of the bioorthogonal reaction depends not only on the click reactivity of the partners, but also on many other factors that typically govern the interaction of NPs with cell surfaces. The physicochemical properties of the NPs, including their size, shape and surface charge have a significant impact on the way they interact with cells.[23] For instance, depending on their size, NPs can be functionalized with multiple targeting ligands to promote a multivalent binding to cell surface receptors, and this can ultimately dictate the NP uptake and subcellular localization.[24] Furthermore, the exposure of NPs to biological environments can trigger the unspecific adsorption of biomolecules (mainly, proteins) onto their surface. This effect is known as protein corona formation and can have a negative effect on the bioorthogonal reactivity of NPs, due to steric hindrance.[25] All these factors emphasize the importance of an appropriate surface engineering of the NPs to ensure a high performance in terms of bioorthogonal reactivity for biological applications. Moreover, prior to cell work, it would be advisable to perform a systematic assessment of the reactivity in different scenarios mimicking the cellular environment.

In this work, we developed a systematic study of the bioorthogonal reactivity of the MNPs from their aqueous suspension state to their final application in biological media. Taking as starting point our previous work on clickable MNPs,[26] spherical MNPs of 13 nm in diameter were firstly functionalized with two different passivation agents, poly(ethylene glycol) (PEG) and a glucopyranoside derivative (GLC), to study how the protein corona could affect the MNP stability and the cell-MNP interaction. Secondly, we introduced two different strained alkyne molecules, a

cyclooctyne derivative (CO) and a dibenzocyclooctyne derivative (DBCO) on the MNP surface to form a triazole ring through the bioorthogonal SPAAC reaction. Using azides as bioorthogonal reaction partners, we assessed the reactivity of the CO- and DBCO-MNPs in suspension and quantified their covalent binding to azide-labelled surfaces, both in water and cell culture medium conditions. Third, we optimized and compared the expression of azide reporters on living cell membranes using three different cell lines (human breast adenocarcinoma, MCF7; human colorectal carcinoma, HCT116 and human lung carcinoma, A549). Finally, we assessed the MNP reactivity against azide-tagged living cells, confirming their covalent binding.

Results and discussion

MNP synthesis and physicochemical characterization

In this work, we have prepared and evaluated the bioorthogonal click reactivity of four different magnetic nanoparticles suitable for SPAAC chemistry (Scheme 1). We have tested two different surface passivation strategies, using 4-aminophenyl β-D-glucopyranoside (GLC, **1**) and amino-polyethylene glycol (PEG, **2**) derivatives, as well as two different strained alkyne derivatives – cyclooctynylamine (CO) **3** and dibenzocyclooctynylamine (DBCO) **4** (Scheme 1). The choice of the surface passivating agents was dictated on the one hand by previous results from our group showing that *in vitro* fate and cellular internalization kinetics of nanoparticles are heavily influenced by the surface functionality,[27] and on the other hand by our preliminary work with cyclooctynylamine **3**-decorated MNPs, in which MNPs modified with GLC were found to react more efficiently with azide-modified substrates than their PEG counterparts.[26] Regarding the selection of the strained alkynes, we have previously reported the synthesis of molecule **3**, a simple cyclooctynylamine derivative bearing a short ethylene glycol chain.[26] This molecule has the advantage of a good stability in aqueous solution, which makes it an attractive candidate for the

functionalization of nanoparticles for biological applications; however, it is known that simple cyclooctynes display slower reaction kinetics when compared to more complex ones, for example those including additional strain elements, such as dibenzocyclooctyne derivatives.[18,28,29]

Therefore, our aim was to compare cyclooctynes **3** and **4** in terms of ease of MNP functionalization, colloidal stability of the functionalized MNPs and click reactivity once attached to the MNP surface.

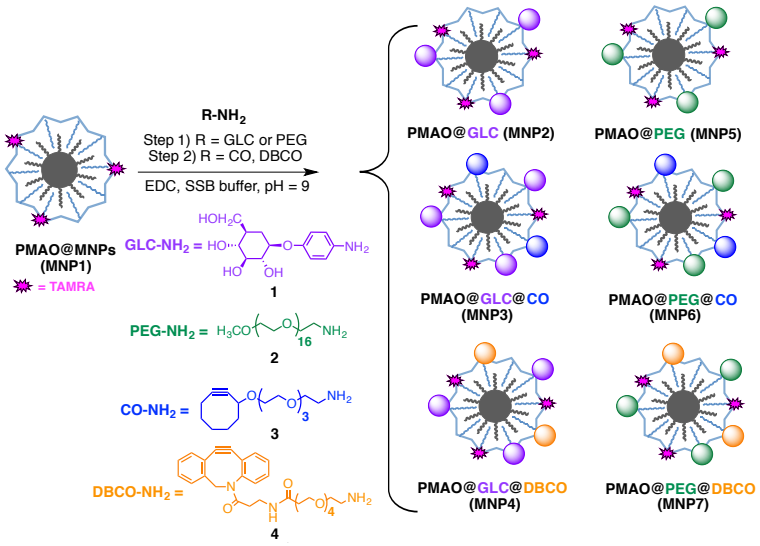

Scheme 1. Preparation of the different MNP families.

Monodisperse spherical iron oxide nanoparticles with a mean diameter of 13 nm were obtained in organic phase by thermal decomposition of iron acetylacetonate $Fe(acac)_3$ and transferred to water by coating with an amphiphilic polymer (poly(maleic anhydride-*alt*-1-octadecene) - PMAO), as previously reported.[26,30] Prior to the water transfer step, the polymer was modified with a TAMRA (5(6)-carboxytetramethylrhodamine) derivative, namely 5(6)-TAMRA cadaverine, to allow the analysis of the MNPs by fluorescence microscopy and flow cytometry.[27] The PMAO-coated MNPs were then functionalized stepwise with GLC, PEG and the two cyclooctynyl derivatives (see Table S1 and Table S2). TEM images (Figure 1A) revealed no morphological

changes of the PMAO-coated MNPs after functionalization, in line with our previous observations. The correct functionalization of the MNPs was verified after each step by agarose gel electrophoresis (Figure S1 in the Supporting Information, SI), ζ-potential measurements (Figure 1C, Figure S1) and thermogravimetric analysis (TGA, Figure 1D). The change in the ζ-potential values from -33 mV for the PMAO-coated MNPs to less negative values was consistent with a reduction of the number of COOH groups available on the surface of the MNPs and was corroborated by a decrease in the electrophoretic mobility in the agarose gel. TGA analysis provided some important insights into the extent of functionalization after each step, revealing nearly equal densities of PEG and GLC ligands per surface unit of MNP (2.8 PEG/nm^2 and 2.6 GLC/nm^2, corresponding to approximately 1250 PEG ligands and 1160 GLC ligands per MNP, respectively). Moreover, similar densities were also estimated for the different strained alkyne moieties (1.7 and 1.3 CO molecules/nm^2 and 0.7 and 1.2 DBCO molecules/nm^2 for PEG and GLC-coated MNPs, respectively; see Table S6 and section 10 in the SI for more details). The slightly lower extent of functionalization with DBCO molecules in the case of PEG-coated MNPs can be attributed to the larger size of the DBCO molecule, in combination with the higher steric hindrance exerted by the PEG ligands over the free carboxyl reactive groups of the MNPs.

All functionalized nanoparticles showed good colloidal stability in water and physiologically relevant media (Dulbecco's modified Eagles' medium, DMEM and DMEM supplemented with 10 % fetal bovine serum, FBS), as revealed by dynamic light scattering (DLS) measurements of the hydrodynamic diameter of the MNPs in each medium (Figure 1B), as well as visual inspection of the MNP suspensions (see Figure S2). In contrast, MNPs coated only with PMAO were stable in water due to their highly negative charge, but aggregated in DMEM and serum-containing DMEM, due to the electrostatic imbalance induced by the different ions present in DMEM (e.g.,

Ca^{2+}, K^{+}, Na^{2+}, SO_4^{2-}, Cl^{-}, etc.) and the adsorption of serum proteins with the subsequent formation of the so-called "protein corona".[31]

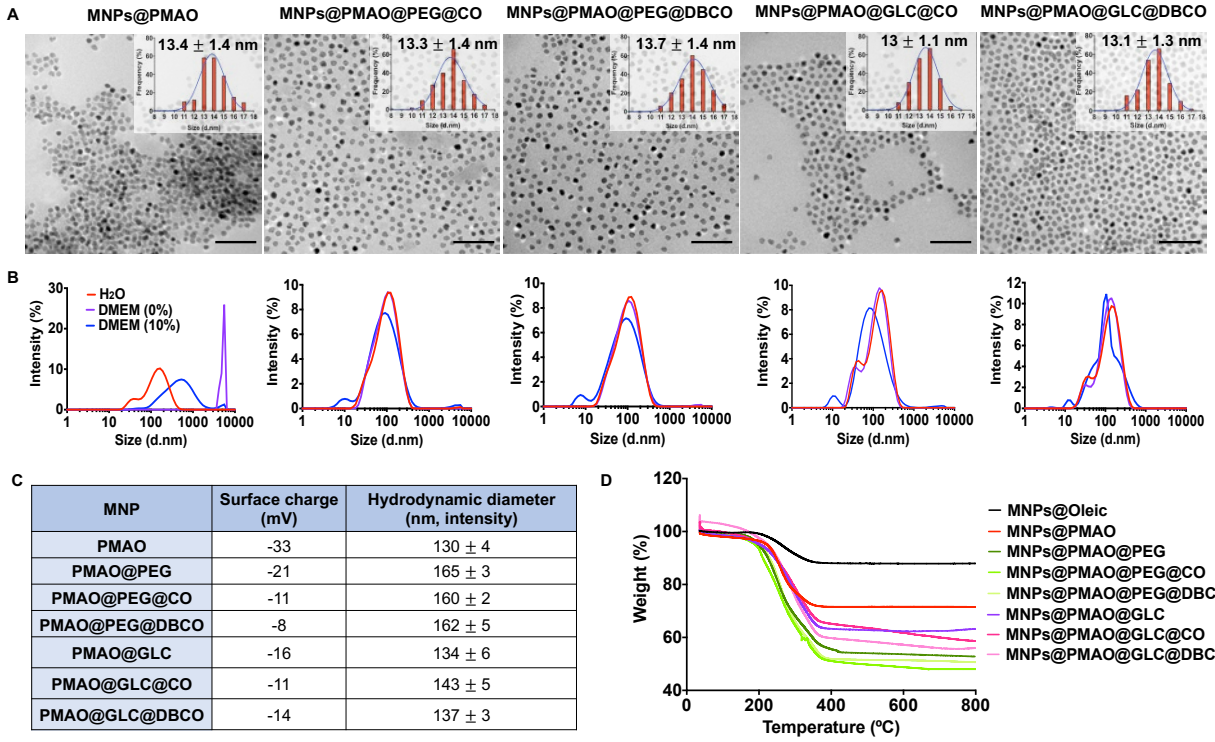

MNP	Surface charge (mV)	Hydrodynamic diameter (nm, intensity)
PMAO	-33	130 ± 4
PMAO@PEG	-21	165 ± 3
PMAO@PEG@CO	-11	160 ± 2
PMAO@PEG@DBCO	-8	162 ± 5
PMAO@GLC	-16	134 ± 6
PMAO@GLC@CO	-11	143 ± 5
PMAO@GLC@DBCO	-14	137 ± 3

Figure 1. Physicochemical characterization of the clickable MNPs. (A) Morphology and size distribution analysis by TEM. Scale bar is 100 nm. (B) Dynamic light scattering measurement of the hydrodynamic diameter of the different MNPs in water, DMEM and DMEM supplemented with 10 % FBS. (C) Surface charge and hydrodynamic diameter values for the MNPs in water. (D) Thermogravimetric analysis curves of the MNPs with different surface coatings.

"Click" reactivity of the MNPs with azides in suspension

We next assessed the reactivity of the strained alkyne moieties present on the MNP surface towards azides in suspension. These experiments would also indicate whether the immobilization of the cyclooctynes on the MNPs affects their reactivity and/or availability (e. g., by possible steric hindrance exerted by the polymer coating or by the passivating molecules, especially the PEG). We first conducted a SPAAC reaction between the MNPs functionalized with strained alkynes and

an azide-modified PEG (PEG-N_3, MW 5000 Da); we reasoned that the large molecular weight of the PEG-N_3 would lead to a drastic change in the electrophoretic mobility of the nanoparticles in the agarose gel. As it can be inferred from Figure S3, for the MNPs functionalized with DBCO we observed larger changes in the electrophoretic mobility when compared to their CO counterparts; this seems to suggest a higher reactivity of the DBCO, in accordance with previous reports.[28,29] This superior reactivity of DBCO is more evident at lower "click" reaction times (30 min). We also tested the "click" reactivity of the MNPs in a fluorogenic SPAAC reaction with 3-azido-7-hydroxycoumarin, a molecule in which the fluorescence emission is quenched due to substitution with azide at the 3- position.[32] Upon the formation of the triazole ring, the fluorescence is restored, indicating the success of the SPAAC reaction. In line with the results obtained in the reaction with PEG-N_3, we have again observed a faster reaction when using nanoparticles functionalized with DBCO. Figure 2 shows the fluorescence intensity variation as a function of the reaction time for the four strained alkyne-functionalized MNPs incubated for 6 h at 37 °C with increasing concentrations of 3-azido-7-hydroxycoumarin (from 0 to 300 μM) in H_2O. ~~While for both PEG@DBCO and GLC@DBCO MNPs the SPAAC reaction was completed in approximately 1 h, the PEG@CO and GLC@CO MNPs required much longer reaction times, of up to six hours.~~ For both PEG@DBCO and GLC@DBCO MNPs, the variations in the fluorescence intensity post-SPAAC reaction were maximized during the first two hours of reaction, for most of the concentrations of 3-azido-7-hydroxycoumarin tested. In contrast, the PEG@CO and GLC@CO MNPs required much longer reaction times, of up to six hours. Moreover, for a given time and 3-azido-7-hydroxycoumarin concentration, the fluorescence intensity observed for the CO-functionalized MNPs was always lower than for the DBCO-functionalized MNPs, thus corroborating the faster kinetics of DBCO. This set of experiments also revealed that the strained

alkyne moieties reacted slower when attached to the nanoparticle surface than in solution (see Figures S4 and S5 in the SI for the fluorescence intensity graphs corresponding to the fluorogenic reaction between 3-azido-7-hydroxycoumarin and free strained alkynes **3** and **4**). This can be attributed to a lower availability of the strained alkyne moieties due to conformational changes or steric hindrance exerted by the PEG and GLC ligands. The results obtained from the fluorogenic click also allowed us to obtain an estimation of the number of CO and DBCO molecules per MNP (see SI): in the case of CO, 3.1 and 2.7 CO molecules/nm^2 were estimated for MNPs@PEG@CO and MNPs@GLC@CO respectively, while for the DBCO, the values were of 0.8 and 0.7 DBCO molecules/nm^2 for MNPs@PEG@DBCO and MNPs@GLC@DBCO, respectively. These values were of the same order of magnitude as the ones obtained from TGA data. Furthermore, we investigated if the "click" reactivity of the MNPs was affected by cell culture conditions, which means the presence of additional biomolecules, ions, and proteins in the reaction medium. Fluorescence emission spectra after 1 h of reaction at 37 °C in DMEM (0 % FBS) and DMEM (10 % FBS) confirmed that the reactivities of the four cyclooctyne-functionalized MNPs were similar to the ones observed in water, suggesting the appropriateness of our MNPs for bioorthogonal reactions in complex media (see Figure S6 in the SI).

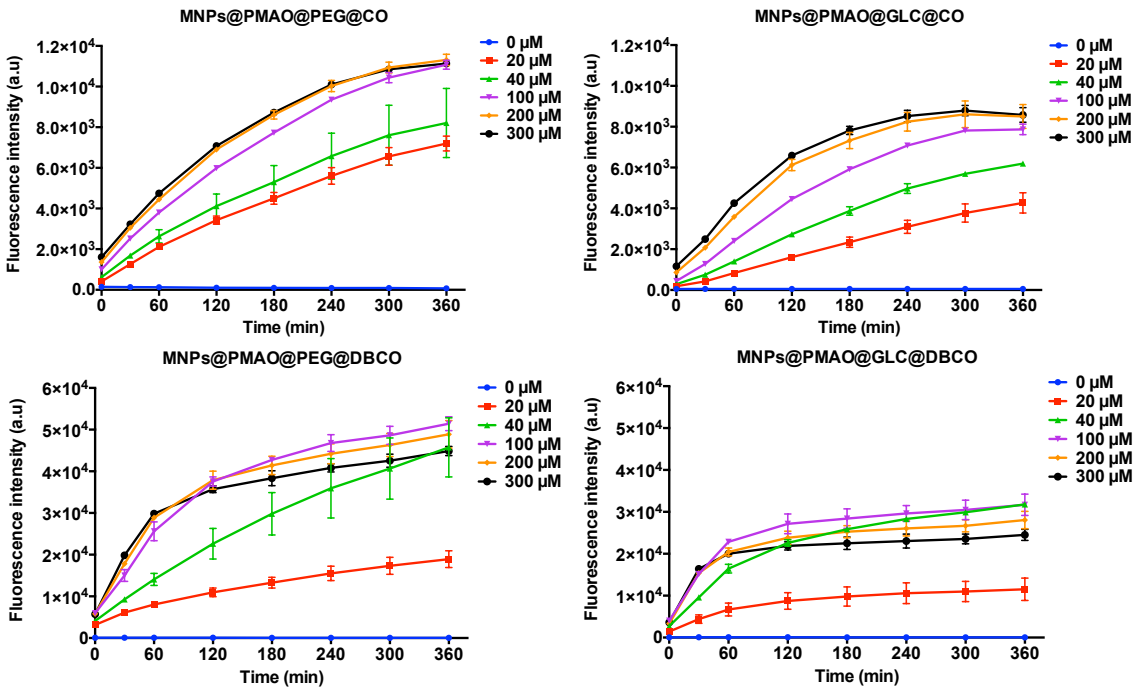

Figure 2. Fluorogenic SPAAC reaction between strained alkyne-functionalized MNPs (60 µg/mL) and 3-azido-7-hydroxycoumarin (0-300 µM) in H_2O. The evolution of the fluorescence emission at 460 nm was monitored during 6 h.

"Click" reactivity of the MNPs towards surface-immobilized azides

While the experiments discussed in the previous section provided useful insights into the reactivity of the CO and DBCO moieties, the assessment of the behavior of our "clickable" MNPs towards azide immobilized on surfaces would be more representative for the final application scenario in which the MNPs would be attached to the membrane of azide-labelled cells. To this end, we conducted a comparative study of the nanoparticle reactivity using quartz crystal microbalance (QCM) substrates modified with azide groups. The QCM is widely used as a biosensing platform operating on the piezoelectric effect and correlating changes in the resonant frequency of the crystal with the mass of material deposited onto the crystal surface.[33,34] QCM-based biosensors typically display high sensitivity, being able to detect very low surface mass

changes (in the range of nanograms/cm^2). Therefore, we envisaged that QCM would be an ideal technique to analyze the difference between the "click" reactivities of our MNPs. To introduce azide groups onto the surface of the QCM substrates, we took advantage of the ease of functionalization of gold surfaces through the formation of thiolated self-assembled monolayers (SAMs).[35,36] A two-step functionalization protocol based on the formation of a monolayer of 11-bromo-undecanethiol and subsequent nucleophilic substitution of the terminal bromine by azide was followed (Figure 3). The correct functionalization of the gold substrate was confirmed using two different techniques: water contact angle measurement and X-ray photoelectron spectroscopy (XPS). Contact angle measurements were performed in two different regions of each substrate, in order to confirm the homogeneity of the functionalization. The results revealed a considerable increase of the contact angle after the first functionalization step, due to the increase of the hydrophobicity of the gold once the 11-bromo-undecanethiol monolayer was incorporated (from 52° for bare gold to approximately 77° for the bromine-modified surface). In the second step, the contact angle was slightly lower (71°), indicating the successful substitution of the Br by N_3. XPS analysis also revealed the correct functionalization with 11-bromo-undecanethiol in the first stage and the complete substitution of the terminal bromine by azide (Figures S7, S8 and S9 in the SI). With the azide-functionalized QCM substrates in hand, we next studied their SPAAC reaction with MNPs bearing strained alkyne moieties (Figure 3) and quantified the mass changes due to "click" reactions.

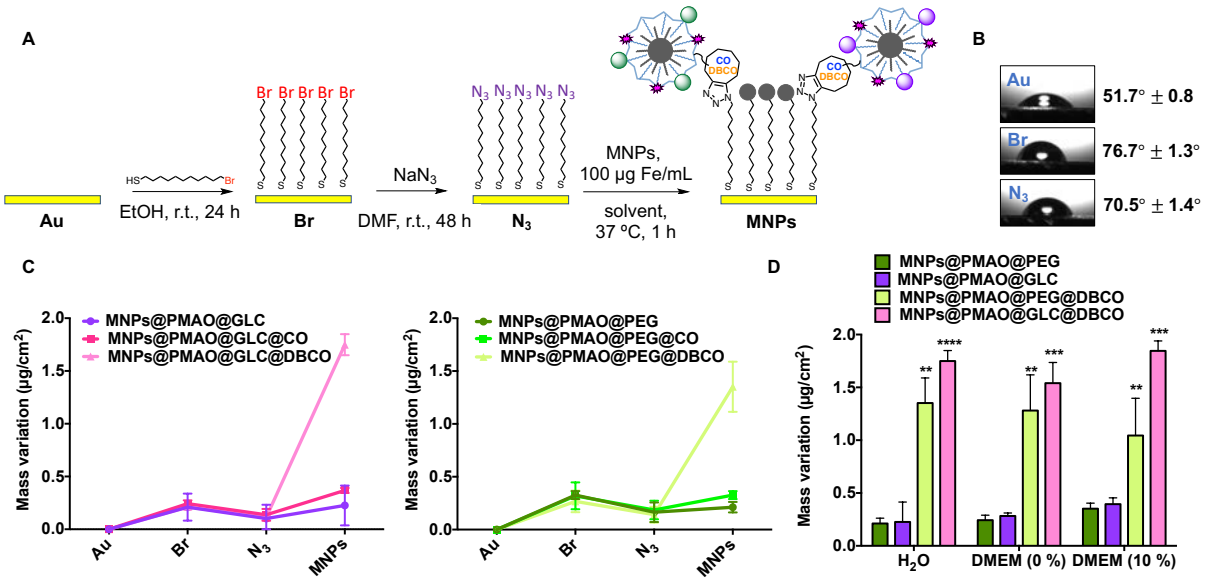

Figure 3. QCM experiments of the reactivity of the MNPs towards surface-immobilized azides. (A) Functionalization strategy of Au substrates with terminal azide groups. (B) Water contact angle measurements on each functionalization step. (C) QCM measurements on each functionalization step and after the incubation of MNPs for 1 h at 37 °C in H_2O. (D) Comparison of the MNPs attachment after 1 h at 37 °C in H_2O, DMEM (0% FBS) and DMEM (10% FBS). Black asterisks indicate statistical differences with respect to the control MNPs@PMAO@PEG or MNPs@PMAO@GLC for each incubation condition (*$p < 0.1$; **$p < 0.01$; ***$p < 0.001$; two-way ANOVA, Tukey's multiple comparisons test). Data analyses are expressed as mean ± SD of two independent experiments.

Taking into account the results obtained in the fluorogenic "click" reaction with 3-azido-7-hydroxycoumarin, we chose to incubate the QCM substrates for 1 h at 37 °C with aqueous suspensions of 100 µg/mL of the different types of MNPs. From the mass variations registered, using the Sauerbrey equation (see SI), we could clearly identify two main reactivity features of our MNPs. First and foremost, in line with the behaviour observed in suspension, the selected cyclooctyne played a key role in the interaction at surface level, the mass variation detected in the

case of MNPs@PEG@DBCO and of MNPs@GLC@DBCO being up to four times higher than the one observed for the CO counterparts. Second, regardless of the passivating agent used, the reactivity of the MNPs was very similar for the same type of strained alkyne. The slightly higher mass variation observed for the MNPs@GLC@DBCO with respect to their PEG analogue was attributed to a higher exposure of the DBCO moiety due to the smaller size of the surrounding GLC molecules in comparison to the PEG. Moreover, due to the fact that the mass of the PEG or GLC-coated MNPs is not exactly the same, the estimation of the MNPs immobilized per unit of area confirmed a slightly higher density of immobilized MNPs@GLC@DBCO with respect to MNPs@PEG@DBCO (see SI for detailed calculations). In addition, both types of control nanoparticles (MNPs@GLC and MNPs@PEG) presented minimal non-specific interactions with the azide-functionalized substrates, indicating a good passivation of the MNP surface with GLC and PEG. Finally, to mimic the final *in vitro* scenario and assess the "click" reactivity in biologically relevant media, the DBCO-functionalized MNPs, which were the ones that displayed the higher reactivity in previous tests, were evaluated in cell culture conditions with and without FBS. Furthermore, to verify that a possible non-specific adsorption of serum proteins on the substrate was not overexpressing the mass variation registered, MNPs@PEG and MNPs@GLC were tested as controls. To our delight, the mass variations observed were very similar to those obtained when the reaction was conducted in water, thus confirming that the SPAAC reaction occurred efficiently even in biological environments (Figure 3D). Based on all the results obtained so far, only the MNPs@PEG@DBCO and MNPs@GLC@DBCO were selected for the labelling of living cell membranes.

Click" reactivity of the MNPs towards cell membrane glycoproteins labelled with azide groups

The results discussed in the previous sections clearly pointed out in the direction of a superior reactivity of the DBCO-modified nanoparticles. Therefore, we expected a similar behavior in terms of interaction of the MNPs with cells expressing azide bioorthogonal reporters on their membranes. These azide reporters were introduced via metabolic glycoengineering, by incubating MCF7, HCT116 and A549 cells with tetraacetylated N-azidoacetylmannosamine (Ac_4ManNAz).[37,38]

A main advantage of the metabolic glycoengineering approach is that it allows the introduction of unnatural receptors (such as the azide groups) on the cell surface in a dose-dependent manner, by incubating the cells with different amounts of the metabolic precursor, in this case Ac_4ManNAz. This azide-modified monosaccharide is hydrolyzed to *N*-α-azidoacetylmannosamine (ManNAz) by cytosolic esterases and finally incorporated into the cell's glycocalyx as *N*-azidoacetyl sialic acid. Indeed, treatment of studied cells during 48 h with increasing concentrations (0-150 μM) of the azide precursor, followed by SPAAC labelling during 30 min with 20 μM of DBCO-modified fluorescent probes sulforhodamine B (Figure S10) and Alexa Fluor 488 (Figure 4A), produced increasingly higher cell membrane fluorescence signals. This confirms the presence on the glycocalyx of unnatural sialic acids containing azide moieties. The dose-dependent generation of azides was also confirmed by western blot (WB) analysis of proteins extracted from cells treated with Ac_4ManNAz (Figure 4B and S11). Previous studies have shown that the metabolic conversion of azide-modified monosaccharides into unnatural cell surface sialosides can vary among different cell lines.[39,40] For this reason, the time- and concentration-dependent generation of azide groups on the surface of the three cell lines tested was carefully evaluated using flow cytometry and WB

analysis. Cells were incubated with different concentrations of Ac_4ManNAz for 24 to 72 h prior to being labelled with DBCO-AF488 *in vivo* or after the extraction of proteins for WB analysis.

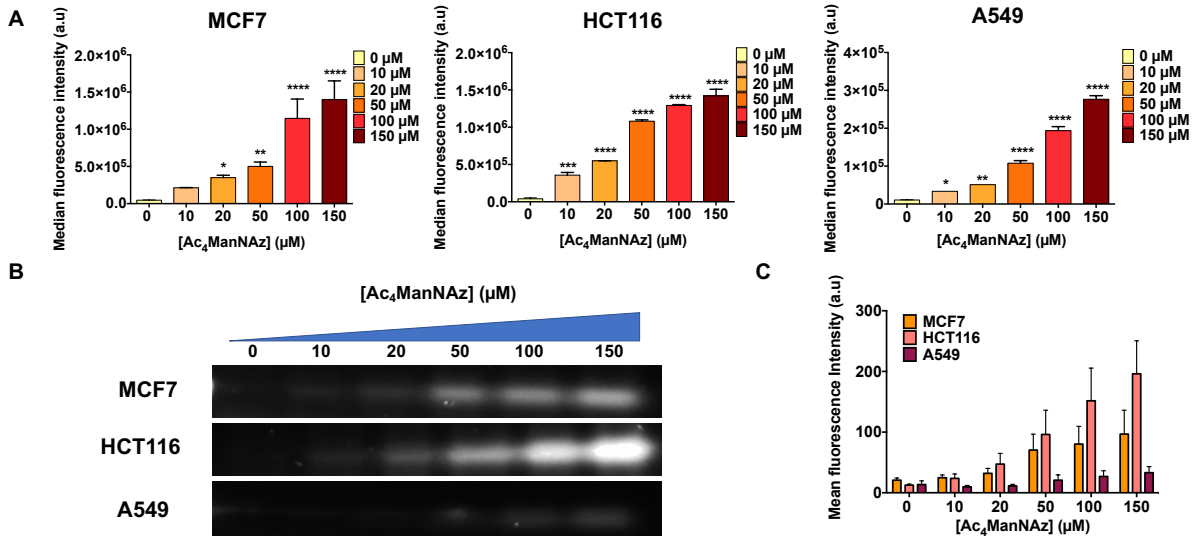

Figure 4. Generation of azide groups on cell membranes using metabolic glycoengineering. (A) Fluorescence intensity detected by flow cytometry of cells treated with different concentrations of Ac_4ManNAz (0, 10, 20, 50, 100, 150 μM) for 48 h in MCF7 and HCT116 and 24 h in A549, followed by 30 min incubation with 20 μM of DBCO-AF 488. Black asterisks indicate statistical differences with respect to the control cells without Ac_4ManNAz treatment (*$p < 0.1$; **$p < 0.01$; ***$p < 0.001$; one-way ANOVA, Dunnett's multiple comparisons test). Data analyses are expressed as mean ± SD of two independent experiments. (B) Western blot (WB) analysis of the azide groups after incubation of MCF7 and HCT116 cells with increasing concentrations of Ac_4ManNAz (0, 10, 20, 50, 100, 150 μM) for 48 h in MCF7 and HCT116 and 24 h in A549, followed by 1 h incubation with 20 μM of DBCO-AF 488. (C) Image analysis of WB bands and comparison of the three cell lines.

Our results revealed different time-dependent azide expression levels for each cell line, with optimal values at 48 h in MCF7 and HCT116 cells and at 24 h in A549 cells (Figure S12 in the SI). A549 cells exhibited ten times lower azide expression comparing with the other two cell lines studied, even at the highest Ac_4ManNAz concentrations tested. Although the strongest signal was observed for the highest concentration of Ac_4ManNAz (150 μM) on the three incubation times tested, the optimal concentration for metabolic glycoengineering was ultimately selected based on a careful evaluation of the cytotoxicity of this compound on the three cell lines. At low azidosugar concentrations (below 50 μM), no apparent cytotoxic effects were observed when assessing metabolic activity, cell morphology and growth rates (see Figures S13-S17 in the SI). However, higher concentrations and prolonged incubation with Ac_4ManNAz impacted the MCF7 and HCT116 cells in terms of cell growth and metabolic activity, with HCT116 cells being more sensitive to high concentrations and 72 h incubation time. These observations are in line with previously reported physiological effects of unnatural azidosugars used for metabolic glycoengineering on A549 cells,[41] progenitor endothelial cells[42] and stem cells.[19] Based on these results, we selected as optimal metabolic glycoengineering conditions a concentration of Ac_4ManNAz of 100 μM for MCF7 cells and of 50 μM for HCT116 (at these concentrations, the cell viability, as inferred from the MTT assays, was similar for both cell lines) and an incubation time of 48 h. These conditions ensure a proper installation of azide reporters on the cell membrane, without compromising the cell viability. Since in A549 cells the metabolic glycoengineering was much less efficient than in the other two cell lines tested, they were discarded for further evaluation of the bioorthogonal reactivity of MNPs.

Finally, once the optimal conditions for the expression of azides were determined, the half-life time of these artificial reporters on the cell membrane was evaluated using live-cell time-lapse

fluorescence microscopy. Results showed that the amount of azide groups present on the membrane gradually decreased due to the membrane turnover.[19,43] At around 6-8 h in MCF7 cells and 4-6 h in HCT116, we started to observe a clear internalization of the azide labelled glycoproteins (Figure S18 and S19 in the SI). This information is crucial, as it determines the timeframe for performing the bioorthogonal "click" reaction of the MNPs onto the membrane after the treatment with Ac_4ManNAz.

Prior to the bioorthogonal "click" immobilization of the MNPs on the cell membranes, the potential cytotoxicity of the nanoparticles was evaluated by MTT assay. MCF7 and HCT116 cells were incubated with MNPs@PMAO@PEG@DBCO and MNPs@PMAO@GLC@DBCO, at concentrations ranging from 25 to 200 μg Fe/mL in cell culture conditions (Figure S20 and S21 in the SI). Two incubations times (24 and 48 h) were tested to evaluate short- and mid-term cytotoxic effects derived from their intrinsic cellular internalization in terms of cell proliferation and metabolic activity. Cell viability values above 90% were obtained for both cell lines at concentrations below 100 μg/mL. However, the cell viability decreased dose-dependently from 85 % to 74.5 % in HCT116 and from 90 % to 80 % in MCF7 when the concentration of MNPs increased from 150 μg Fe/mL to 200 μg/mL at 48 h of incubation. No significant differences were observed between the different types of MNP surface functionalization, thus allowing us to assume a dose-dependent cytotoxic effect. Therefore, 100 μg/mL of MNPs was selected as an optimal concentration for further experiments.

The "click" reactivity of MNPs@PMAO@PEG@DBCO and MNPs@PMAO@GLC@DBCO towards azide-labelled living cell membranes was initially evaluated using fluorescence microscopy. According to the optimal conditions established before in suspension and using azide-functionalized gold surfaces, MNPs were incubated for 1 h in cells with (N_3+) and without

Ac_4ManNAz (N_3-) treatment. After the reaction, the excess of MNPs was discarded and cells were washed twice with DPBS to remove the unbound MNPs. An effective MNP immobilization on the cell membrane was clearly observed, but unspecific interactions of the MNPs with the membranes of cells not treated with Ac_4ManAz were also detected. By quantifying the mean fluorescence intensity, narrow differences between N_3+ and N_3- cells were found, which led us to conclude that fluorescence microscopy is not a suitable technique to assess the efficiency of the "click" reaction (see Figure S22). This is mainly because of the small size of MNPs (13 nm) and the resolution limits for the detection of individual MNPs homogeneously distributed along the whole cell membrane, which is better suited for super-resolution microscopy.[44] For this reason, the quantitative analysis of fluorescence intensity was addressed using flow cytometry. The MNP reactivity was tested in both cell lines by incubation for times varying from 30 min to 24 h (Figure S23. At each time point, the unbound MNPs were discarded by washing the cells twice with PBS, then cells were detached with a non-enzymatic agent (Versene®) to avoid the loss of covalently attached MNPs onto cell membrane azide-tagged glycoproteins, and the cells were analyzed by flow cytometry recording the fluorescence signal of TAMRA. MNPs were preferentially conjugated to N_3+ cells, as demonstrated by the data obtained after only 30 min of incubation. Moreover, the longer the incubation time, the higher was the non-specific interaction of MNPs with N_3- cells.

Considering 1 h of MNP incubation as the optimal time for the click reactivity without having extensive non-specific MNPs interaction derived from prolonged incubation times, the effect of the density of azide bioorthogonal reporters on cell membrane was evaluated. For this purpose, the binding of MNPs onto cells dose-dependently treated with Ac_4ManNAz (25 μM to 100 μM) was evaluated (Figure 5A). Results revealed a slight increase in the efficiency of the click reaction with

increasing Ac_4ManNAz concentration for both cell lines and both types of MNPs. These results confirmed the bioorthogonal click reaction in physiological conditions. Furthermore, taking into account the difficulties encountered when using fluorescence microscopy to assess the immobilization of the MNPs on cell membranes via SPAAC chemistry, transmission electron microscopy was used to obtain a general idea regarding the distribution of the MNPs on the membrane (Figure S24 in the SI).

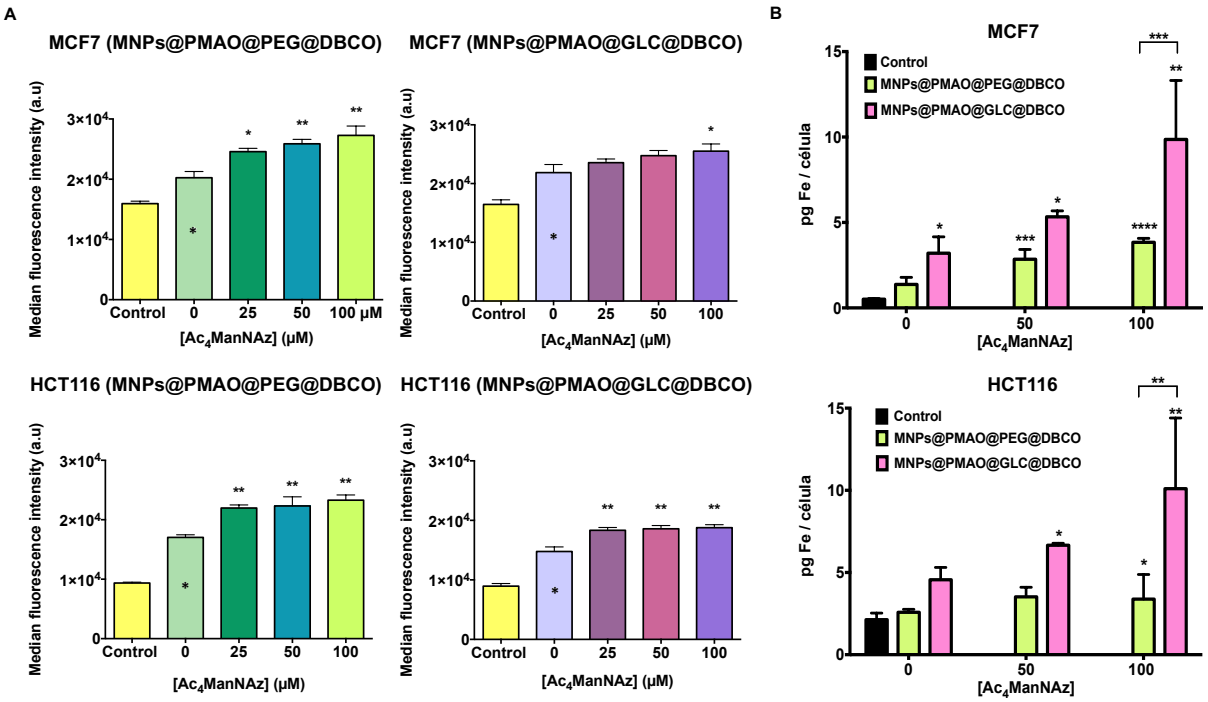

Figure 5. (A) Flow cytometry measurements after 1 h of reaction of MNPs@PMAO@PEG@DBCO and MNPs@PMAO@GLC@DBCO in MCF7 and HCT116 pre-treated with Ac_4ManNAz (0, 25, 50 and 100 μM) for 48 h. Black asterisks indicate statistical differences with respect to control cells without MNP and Ac_4ManNAz treatment (0 μM) (*$p < 0.1$; **$p < 0.01$; one-way ANOVA, Dunnett's multiple comparisons test). (B) Iron content per cell quantified by ICP-AES after 1 h of reaction of MNPs@PMAO@PEG@DBCO and MNPs@PMAO@GLC@DBCO in MCF7 and HCT116 pre-treated with Ac_4ManNAz (0, 50 and

100 μM) for 48 h. Black asterisks indicate statistical differences with respect to control cells without MNP and Ac_4ManNAz treatment (*$p < 0.1$; **$p < 0.01$; ***$p < 0.001$; two-way ANOVA, Tukey's multiple comparisons test).

Finally, we turned our attention towards a more sensitive technique for a total quantification of the iron content per cell after the click reaction, namely inductively coupled plasma atomic emission spectroscopy (ICP-AES). Following the same MNP incubation strategy described before, the amount of iron (Fe) in cells treated with different Ac_4ManNAz concentrations (0, 50 and 100 μM) was quantitatively determined using ICP-AES (Figure 5B). Results confirmed an efficient SPAAC reaction, directly proportional to the azide density on the cell membrane for both cell lines studied. Even more, a higher binding of MNPs@PMAO@GLC@DBCO was detected on each Ac_4ManNAz concentration and for both cell lines with respect to the PEG analogues. In MCF7 cells treated with 100 μM of Ac_4ManNAz 10 pg Fe/cell were detected for MNPs@PMAO@GLC@DBCO, compared to only 3.8 pg Fe/cell for MNPs@PMAO@PEG@DBCO. Similarly, in HCT116 cells approximately 7 pg Fe/cell were detected for MNPs@PMAO@GLC@DBCO and only 3.5 pg Fe/cell for MNPs@PMAO@PEG@DBCO at the optimal Ac_4ManNAz concentration of 50 μM. These differences between the two types of MNPs that passed unnoticed in flow cytometry experiments can be explained from two perspectives. The first one is related to the intrinsic fluorescence of PEG, with an excitation peak between 488 and 550 nm and an emission peak at 580 nm (see Figure S25 in the SI). ~~This effect leads to a lower fluorescence intensity of the MNPs functionalized with GLC for the flow cytometer detector and subsequently underestimates the overall signal of the real amount of MNPs immobilized on cells.~~ This effect leads to a higher fluorescence intensity of the MNPs functionalized with PEG for the flow cytometer detector and subsequently overestimates

the overall signal of the real amount of PEG-MNPs immobilized on cells. The second one could be related to the higher exposure of the DBCO moieties on the surface of the GLC-coated MNPs in comparison to the PEG analogues, in line with the results obtained in the QCM experiment onto gold azide-functionalized surfaces. Overall, these results allowed us to confirm the cell surface engineering of living cells with MNPs using SPAAC.

Conclusions

In this work, we described a systematic approach for assessing the bioorthogonal reactivity of four types of MNPs for immobilization on~~to~~ living cell membranes using SPAAC chemistry. ~~Four types of MNPs were prepared, functionalized with two types of passivating agents (PEG and GLC) and two types of cyclic-strained alkynes (CO and DBCO), respectively. The MNPs have been firstly characterized in terms of physico-chemical characteristics, colloidal stability and click reactivity in suspension. In a second step, the~~ The reactivity of the MNPs was ~~first~~ evaluated first in suspension and then towards azide-modified surfaces ~~was evaluated~~, as a closer approach to their final application in a living cell scenario. Finally, based on these initial evaluations, the ~~MNPs@DBCO~~ best MNP candidate ~~were~~ was selected for cell membrane immobilization via SPAAC bioorthogonal click reaction on the membranes of cells engineered to express azide artificial reporters. To the best of our knowledge, this is the first systematic study reporting the use of bioorthogonal SPAAC click chemistry for attaching MNPs to living cell membranes. We are currently investigating how this approach to cell surface engineering can be used for the development of different biomedical applications (in particular, intracellular delivery mediated by transient changes in cell membrane fluidity through localized magnetic and optical hyperthermia).

We envisage that the proposed methodology could be easily extended to other types of NPs; however, we believe that there are some important aspects to be considered for a successful implementation of this approach. In our opinion, the main "take home messages" are:

1) *Surface functionalization matters*. While in our study both types of passivating molecules (PEG an GLC) were suitable for ensuring the colloidal stability of the MNPs, we found that the GLC-coated MNPs performed better in terms of click reactivity, both in water and in cell culture media. This is due to the smaller size of the GLC ligand when compared to PEG, which can lead to a better exposure of the cyclooctynyl moieties on the MNP surface. Moreover, the functionalization with PEG led to non-expected interferences in fluorescence-based characterization techniques (see also point 4 below).
2) *The choice of the strained alkyne is important*. While the DBCO derivative used in this work reacted faster than the simple cyclooctynylamine derivative **3**, it also displayed a more pronounced hydrophobic character. Therefore, in our case the functionalization of the MNPs with the DBCO derivative required a careful optimization of the reaction parameters, to ensure that the colloidal stability of the resulting MNPs was not affected by the hydrophobicity of the DBCO ligands.
3) *The expression of azides on living cell membranes is cell-line dependent*. Metabolic glycoengineering can provide a universal tool for the installation of azide bioorthogonal reporters on cell membranes, which offers clear advantages over the classical chemical conjugation to pre-existing reactive groups, as mentioned in the Introduction. However, the process should be carefully optimized for each cell line, as specific concentrations and incubation times with azide precursor can be required for an optimal expression of azides on the glycocalyx without affecting cell viability.

4) *Seeing is believing, but if you don't see it, it doesn't mean it's not there*. In some instances, the choice of the most appropriate characterization technique for a specific experiment is not obvious, especially when trying to assess subtle differences. We initially relied heavily on fluorescence microscopy and flow cytometry to assess the immobilization of the MNPs on cell membranes through SPAAC chemistry; however, we found that classical fluorescence microscopy techniques lacked the resolution needed for small particles, while in the case of flow cytometry we had to deal with interferences due to the intrinsic fluorescence of the PEG molecules.

We believe that all these considerations will be useful for researchers working in the field of bioorthogonal applications of nanoparticles.

Materials and methods

Reagents

All commercially available reagents were used as supplied, unless otherwise stated. Iron(III) acetylacetonate, 1,2-hexadecanediol, oleic acid, oleylamine, benzyl ether, poly (maleic anhydride-alt-1 octadecene) (PMAO, MW: 30000–50000 g/mol), N-(3-dimethylaminopropyl)-N'-ethylcarbodiimide hydrochloride (EDC), 4-aminophenyl β-D-glucopyranoside (GLC), sodium azide, 11-bromo-undecanethiol , β-mercaptoethanol and CelLytic MT reagent were purchased from Sigma-Aldrich and Merck. α-Methoxy-ω-amino poly(ethylene glycol) (PEG, MW: 750 Da) and α-azido-ω-amino poly(ethylene glycol) (PEG-N_3, MW: 5000 Da) were purchased from Rapp Polymere GmbH. Tetramethylrhodamine-5-carboxamide cadaverine (TAMRA) was from AnaSpec. Chloroform stabilized with ethanol (Reag. Ph. Eur.), absolute ethanol (99.8 % vol.), sulfuric acid (96 % vol.) and oxygen peroxide (33 % w/v) were from Panreac.

Dibenzylcyclooctyne-PEG_4-NH_2 (DBCO), dibenzylcyclooctyne-PEG_4-5/6-sulforhodamine B (DBCO-sulforhodamine), dibenzylcyclooctyne-Alexa Fluor 488 (DBCO-AF488), 3-azido-7-hydroxycoumarin and tetraacetylated N-azidoacetyl-mannosamine (Ac_4ManNAz) were purchased from Jena Bioscience GmbH. 4-15 % Mini-PROTEAN® TGX™ precast protein gels and Laemmli buffer were purchased from BioRad. Acetone (99 % vol.) and N,N-dimethylformamide (DMF, 99.9 % HPLC grade) were purchased from Scharlau Chemies S.A. Amicon centrifugal filter units (100 kDa MWCO) were purchased from Millipore and 0.2 mm pore size 25 mm diameter cellulose acetate membrane filters were from Chmlab. Quartz crystal microbalance (QCM) substrates of Cr/Au, 5 MHz and 2.54 cm in diameter were purchased from Standford Research Systems. Dulbecco's modified Eagle's medium (DMEM), Phosphate-Buffered Saline (PBS), Dulbecco's Phosphate-Buffered Saline (DPBS), GlutaMAX™, penicillin/streptomycin (100 U/mL) and Versene® were purchased from Gibco. 4′,6-Diamidino-2-phenylindole (DAPI), Hoechst 33342, ProLong™ diamond antifade mountant and 3-(4,5-Dimethylthiazol-2-yl)-2,5-Diphenyltetrazolium Bromide (MTT) were purchased from Invitrogen. Glutaraldehyde (2 % vol.) was purchased from Electron Microscopy Sciences. Buffers were prepared according to standard laboratory procedures. Milli-Q water (resistivity of 18.2 MΩ/cm at 25 °C) was obtained using Milli-Q® Advantage A10 system.

Instrumentation

Detailed information on the equipment and instrumentation techniques used is provided in the SI.

MNP synthesis and functionalization

Hydrophobic 13-nm diameter iron oxide nanoparticles were obtained by thermal decomposition of iron acetylacetonate and transferred to water by coating with poly(maleic anhydride-*alt*-1-

octadecene) (PMAO, MW 30000–50000 g/mol, modified with TAMRA fluorophore), as previously described in our laboratory. The functionalization of the MNPs with GLC, PEG, CO and DBCO derivatives was carried out following our previously described two-step approach. In the case of the functionalization with GLC, the molar ratio of GLC was increased to 30 μmol GLC per 1 mg of Fe for a higher MNP stability. In addition, the ratio DBCO/MNPs was optimized at 0.87 μmol/mg Fe to avoid MNP aggregation in physiological media (see SI, Table S1 and S2). The temperature of each functionalization step was controlled at 37 °C for ensuring reproducibility between different batches. More details regarding the functionalization protocols can be found in the SI.

Click reactions in suspension

Click reaction with PEG-N_3. MNPs at a concentration of 100 μg Fe/mL were incubated with 3 mg of azide-modified PEG (PEG-N_3, MW 5000 Da) in a final volume of 250 μL distilled H_2O. The click reaction between the azide and the MNPs was allowed to proceed at 37 °C with gentle shaking (600 rpm) for 30 min or 5 h. After this time, the unreacted PEG was eliminated by washing twice with 500 μL of milli-Q water in Amicon spin filters with a 100 kDa molecular weight cut-off membrane at 12100 xg during 5 min and then, the MNPs were resuspended in 20 μL of distilled H_2O. Mixtures of 6 μL of MNPs and 2 μL of TBE/Glycerol (1:1) were loaded in an agarose gel (1%) and the electrophoresis was carried out in TBE 0.5x at 120 V for 45 min. The gel was analysed using a Gel Doc™ Ez system from BioRad.

Fluorogenic click reaction with 3-azido-7-hydroxycoumarin. MNPs at a concentration of 60 μg Fe/mL in a final volume of 100 μL were incubated in black 96-well plates with different concentrations of 3-azido-7-hydroxycoumarin (0-300 μM). The fluorescence intensity was measured at 37 °C every 10 minutes for 6 h (excitation at 390 nm and emission at 460 nm) using

a Synergy H1 hybrid multi-modal plate reader from BioTek. Calibration plots based on the fluorogenic SPAAC reaction between 3-azido-7-hydroxycoumarin and free CO and DBCO were used to estimate the number of strained alkynes per MNP (See Figure S6 and S7, SI). This reaction was carried out at a 1:1 molar ratio using different concentrations of azide and alkyne (0-300 μM) following the same protocol as described above for the MNPs and the fluorescence values at which the reaction finished were represented on the plot with a linear regression.

The fluorogenic SPACC reaction was also evaluated in cell culture conditions using DMEM with and without FBS. To avoid the intrinsic emission peak of the culture medium at 460 nm, the reaction was carried out in Eppendorf tubes for 1 h at 37 ºC and a final 3-azido-7-hydroxycoumarin concentration of 200 μM. After this time, the MNPs were separated from the culture medium by centrifugation at 12100 xg for 5 min using Amicon spin filters with a 100 kDa molecular weight cut-off membrane. The MNPs were resuspended in 100 μL of milli-Q water and the fluorescence was measured in black 96-well plates as described before.

Click reactions on surfaces

Functionalization of QCM substrates. Commercial QCM Au/Cr substrates with a resonant frequency of 5 MHz and 2.54 cm in diameter from Stanford Research Systems were first functionalized using a three-step protocol to incorporate azide groups on their surface. Each substrate was immersed in piranha solution (1:3, H_2O_2:H_2SO_4) for 1 min and then rinsed with milli-Q water and dried under a stream of nitrogen to remove any dust and contaminants (*Warning! Piranha solution should be handled with extreme caution. It has been reported to detonate unexpectedly*). Then, the substrates were immersed in a 11-bromo-1-undecanethiol solution (1 mM) in absolute ethanol for 24 h at room temperature. Samples were rinsed twice with milli-Q water and anhydrous ethanol, followed by a drying step under a stream of nitrogen. Subsequently,

the substrates were immersed in a saturated solution of sodium azide in N,N-dimethylformamide (DMF) and incubated for 48 h in the dark at room temperature to replace the bromine with azide. Finally, the substrates were rinsed twice with milli-Q water, DMF and absolute ethanol and dried under a stream of nitrogen.

Water contact angle measurements were made using deionized water with an Attension® Theta Lite contact angle goniometer. The water droplet size was kept consistent between measurements using an automated syringe dispenser. At least two measurements were made on each sample, and there were two replicates for each step of the substrate functionalization process. The contact angle value was reported by the instrument's OneAttension software using an auto non-spherical fit to the liquid–vapor interface. Results are reported as the mean value plus the standard deviation of the four measurements.

The surface chemical compositions after each step of the substrate functionalization process were analyzed by X-ray photoelectron spectroscopy (XPS) on a Kratos AXIS Supra spectrometer equipped with a monochromate Al $K\alpha$ X-ray source ($h\nu$ = 1486.6 eV) operated at 120 W. High-resolution spectra were recorded at pass energies of 160 eV. Measurements were performed in ultra-high vacuum (10^{-9} torr) and with the hybrid-slot mode that allows to analyze an area of 700 x 300 μm approximately. All spectra were corrected using the signal of C1s at 285.0 eV as an internal reference and the following regions were measured: C1s, N1s, Au4f, Br3d, Br3p and S2p.

QCM measurements (QCM2000, Stanford Research Systems) were used to quantify the reaction of the strained alkyne-functionalized MNPs with the azide-modified substrates. Each substrate was incubated in a six-well plate with 2 mL of each type of MNP at a concentration of 100 μg Fe/mL in H_2O, DMEM (0 % FBS) and DMEM (10 % FBS) for 1 h at 37 °C. After the incubation, substrates were rinsed with milli-Q water to discard MNPs attached in a non-specific

manner, dried under a stream of nitrogen and measured. Each type of MNP was measured three times with two replica samples.

***In vitro* studies**

Cells. MCF 7 (human breast adenocarcinoma), HCT 116 (human colorectal carcinoma) and A549 (human lung carcinoma) cells (ATCC, Manassas, VA, USA) were cultured in Dulbecco's modified Eagle's medium (DMEM), supplemented with 10 % FBS, GlutaMAX™ (2 mM) and penicillin/streptomycin (100 U/mL), at 37 °C with 5 % CO_2 in a humidified atmosphere. Cells were confirmed to be free of mycoplasma contamination.

Metabolic glycoengineering

Optimization of Ac_4ManNAz concentration. To generate azide groups on cell membranes, cells were seeded at an appropriate density (according to their growth rates, MCF7: 12 x 10^3 cells/well; HCT116: 8 x 10^3 cells/well; A549: 10 x 10^3 cells/well) onto 12-mm diameter glass coverslips inside standard 24-well plates in 400 µL of supplemented DMEM and grown for 24 h under standard cell culture conditions. The cell culture medium was discarded, and cells were further incubated in DMEM with different concentrations of Ac_4ManNAz (0, 10, 20, 50, 100 and 150 µM) for 48 h. The labelling medium was discarded, and the cells were washed twice with DPBS (PBS with extra Ca^{2+} and Mg^{2+}). Then, cells were incubated during 30 min at 37 °C with serum-free DMEM containing 20 µM DBCO-PEG_4-5/6- sulforhodamine B. Cells were then washed twice with DPBS, fixed with 200 µL of 4 % paraformaldehyde, washed twice with PBS and nuclei were stained with a 0.6 µM dilution of 4′,6-diamidino-2-phenylindole (DAPI). Then, two more washing steps with PBS were performed to remove free DAPI. The coverslips were mounted on glass microscope slides using 6 µL of ProLong®. Fluorescence and confocal microscopy images were acquired with a Nikon Eclipse Ti-e inverted microscope and an Olympus

Fluoview FV10i microscope with a 60x oil immersion objective, respectively. Sulforhodamine B and DAPI fluorophores were laser excited at 559 and 405 nm, respectively. Laser intensity and sensitivity values were optimized and maintained constant for each image capture. Z-stack images were obtained with a 1024 x 1024 resolution and analyzed with the Fiji Software.

Ac_4ManNAz cytotoxicity. *In vitro* cell viability tests were carried out to determine the cytotoxicity of Ac_4ManNAz using the 3-(4,5-dimethylthiazol-2)-2,5-diphenyltetrazolium bromide (MTT) colorimetric assay. Five different concentrations of Ac_4ManNAz (10, 20, 50, 100 and 150 μM) and three different incubation times (24, 48 and 72 h) where tested. Depending on the incubation time tested, MCF7, HCT116 and A549 cells were seeded at different densities (from 10 $x10^3$ to 5 $x10^3$ cells/well) using standard 96-well plates (four replicates per sample). After 24 h of incubation in cell culture conditions, the medium was replaced with 200 μL of fresh medium containing the different concentrations of Ac_4ManNAz and a negative control (non- treated cells). After each incubation time, cells were washed with PBS and fresh medium containing MTT dye solution (0.25 mg/mL in DMEM) was added to each well. 1 h later, the plate was centrifuged at 1250 xg for 20 min using an Eppendorf centrifuge 5810R with an A-4-62 rotor, the supernatant removed, and the formazan crystals solubilized with 100 μL of dimethyl sulfoxide (DMSO). After mixing, the optical density at 570 nm was recorded using a Thermo Scientific Multiskan GO™ microplate reader. The relative cell viability (%) related to control cells without treatment was calculated using the percentage ratio between absorbance of the sample and the absorbance of the control. Experiments were performed in duplicate, and data are represented as the mean value ± the standard deviation.

Bio-physiological effects of Ac_4ManNAz on cell growth and morphology. The growth rate and the impact on cell morphology was evaluated by seeding 6-well plates with $1x10^5$ MCF7

cells/well and $8x10^4$ HCT116/A549 cells/well in 1 mL of supplemented DMEM and incubating them with the same concentrations of Ac_4ManNAz tested above for up to 72 h. At each time point, cellular images were taken with an inverted Nikon Eclipse TE2000-S microscope provided with a digital camera (slight ds-Fi1c) and cells were trypsinized, stained with trypan blue (0.4 %) and counted using a Neubauer chamber.

Optimization of the incubation time. The optimal incubation time of Ac_4ManAz for the expression of azide reporters on cell membranes was evaluated using flow cytometry and western blot.

Flow cytometry analysis. Cells were seeded (MCF7: 1.5 x 10^5 cells/well, HCT116 and A549: 1 x 10^5 cells/well) on standard 6-well plates in 2 mL of DMEM and grown for 24 h under standard cell culture conditions. The cell culture medium was discarded, and cells were further incubated in DMEM with five different concentrations of Ac_4ManNAz (10, 20, 50, 100 and 150 μM) for 24, 48 and 72 h. Cells were labelled with DBCO-AF488 (20 μM) for 30 min at 37 °C. Then, cells were detached with Versene®, a non-enzymatic cell dissociation reagent, and centrifuged at 12100 xg for 15 seconds. Finally, the pellet was resuspended in PBS. All samples were analyzed in a CytoFlex Flow Cytometer (Beckman Coulter) and data interpreted with the CytExpert and Kaluza Software. Experiments were carried out in duplicate.

Western blot analysis. Cells were seeded onto 6-well plates (MCF7: $1.5x10^5$ cells/well, HCT116: $1.2x10^5$ cells/well, A549: $1x10^5$ cells/well) in 2 mL of cell culture medium. After 24 h of growth, cells were treated with different concentrations of Ac_4ManNAz (10, 20, 50, 100 and 150 μM; a control with no Ac_4ManNAz was also included) for 24, 48 and 72 h. After each incubation time, cells were detached by adding 800 μL of Versene® to each well. Cells were pelleted by centrifugation at 12100 xg for 15 seconds and the pellets were lysed in 125 μL of

CelLytic MT reagent for 15 min at 37 °C. The insoluble debris were removed by centrifugation for 15 seconds at 12100 xg. Final soluble protein concentrations were determined by Bradford protein assay to be 2 mg/mL. Then, 40 µL of the lysate was incubated with DBCO-AF488 (20 µL, 20 µM in PBS) for 1 h at 37 °C. Loading buffer was added to each sample, and samples were loaded onto 4-15 % SDS-PAGE gels after heating at 95 °C for 5 min. Electrophoresis was run for 1 h at 160 V and the gel was imaged with a BioRad Gel Doc™ Ez system using an exposure time of 3 seconds for the green fluorescence filter. In parallel, a duplicated gel was stained with Ez-Blue Gel Staining reagent according to the manufacturer's protocol to check total protein loaded and using Precision Plus protein standard (10-250 kDa) for molecular weight estimation.

Half-life time of azide groups on the cell membrane. Cells were seeded (MCF7: 6 x 10^3 cells, HCT116: 5 x 10^3 cells) onto µ-slide 8-well chamber slides from Ibidi® in 400 µL of DMEM and grown overnight in cell culture conditions. Medium was then substituted by fresh medium with 100 µM or 50 µM of Ac_4ManNAz in MCF7 and HCT116, respectively, and incubated for 48 h. Prior to the time-lapse experiment, cells were washed twice with DPBS and incubated for 30 min at 37 °C, light-protected, with serum-free DMEM containing 20 µM DBCO-PEG_4-5/6-sulforhodamine B. Then, nuclei were labelled with 40 µM Hoechst 33342 by incubation in supplemented DMEM for 10 min. The cells were washed twice with DPBS and fresh growth medium without phenol red was added. Time lapse images were obtained with a live cell workstation AF6000 LX from Leica under control of temperature and CO_2 atmosphere. Cell images were obtained every 15 minutes for 24 h and were analyzed with Fiji software.

Bioorthogonal "click" chemistry of MNPs on living cell membranes

MNP cytotoxicity. Cells were seeded (MCF7: 4 × 10^3 cells/well, HCT116: 4 × 10^3 cells/well) in a standard 96-well plate (200 µL/well) and incubated for 24 h in cell culture conditions. Cells

were incubated with five different concentrations (25, 50, 100, 150 and 200 μg Fe/mL) of the different nanoparticles in DMEM, with three replicates per concentration. After 24 h and 48 h of incubation, the wells were washed twice with DMEM to remove the nanoparticles and fresh medium containing MTT dye solution (0.25 mg/mL in DMEM) was added to each well. From this point onwards, the protocol followed was the same as that previously described for Ac_4ManNAz.

MNP – cell interaction. Cells were seeded (MCF7: 16 × 10^3 cells/well, HCT116: 12 × 10^3 cells/well) in a standard 24-well plate (400 μL/well) and incubated for 24 h in cell culture conditions. Medium was then substituted by fresh medium with the optimal concentrations of Ac_4ManNAz (100 μM or 50 μM for MCF7 and HCT116, respectively) and incubated for 48 h. After that, 100 μg Fe/mL of MNPs@PMAO@PEG@DBCO and MNPs@PMAO@GLC@DBCO were incubated for different times (30 min to 24 h) at 37 °C in supplemented DMEM. After each incubation time, cells were washed with PBS twice to remove unbound MNPs and samples for fluorescence microscopy and for flow cytometry were prepared following the protocols previously described. Control experiments using cells without Ac_4ManNAz pre-treatment were performed in a similar fashion.

TEM analysis of MNP – cell interaction. Cells were seeded (MCF7: 12 x 10^3 cells, HCT116: 10 x 10^3 cells) onto 8-well chamber slides from Lab-Tek™ in 400 μL of DMEM and grown overnight in cell culture conditions. After the treatment with Ac_4ManNAz, MNPs at 100 μg/mL were incubated for 30 min at 37 °C in DMEM (0 % FBS). The excess of MNPs was removed, cells were washed with PBS and then with cacodylate buffer (0.1 M) for 5 minutes. Cells were fixed with glutaraldehyde 2 % in cacodylate buffer (0.1 M) for 10 min at 37 °C. The fixative agent was replaced and incubated for two additional hours at RT. Fixed cells were rinsed with phosphate buffer (0.1 M) and kept at 4 °C. Sample sectioning and grid mounting was performed by the

Electron Microscopy Service at the Centro de Investigación Principe Felipe (CIPF, Valencia, Spain).

Inductively coupled plasma – atomic emission spectroscopy (ICP-AES) analysis. Total iron concentration per cell was determined by ICP-AES. For ICP measurements, 150000 - 200000 cells previously treated with 0, 50 and 100 μM Ac_4ManNAz for 48 h were incubated with 100 μg/mL of MNPs@PMAO@PEG@DBCO and MNPs@PMAO@GLC@DBCO for 1 h at 37 ºC in DMEM (0 % FBS). After that, cells were washed twice with PBS and detached with Versene® for 15 min. Pelleted cells were treated with 100 μL of piranha solution for 15 min and 300 μL of aqua regia (3:1, HCl:HNO_3) for 2 h at room temperature, incubated at 60 ºC for 15 min, diluted with milli-Q water to 20 mL and analyzed by ICP-AES (HORIBA Jobin Yvon - ACTIVA-M). Experiments were carried out in triplicate and results represented as the mean value ± the standard deviation.

Statistical analysis

Data were analyzed using GraphPad Prism 6.0 (GraphPad Software, San Diego, USA). The results are represented as the average ± standard deviation of at least two independent experiments. Analysis of variance (ANOVA) with Tukey's or Dunnett's multiple comparisons test were used to evaluate differences between groups and were considered statistically significant at p value < 0.1.

ASSOCIATED CONTENT

Supporting Information.

The Supporting Information is available free of charge and includes a .pdf file containing:

- Instrumentation; Functionalization of MNPs with poly(ethylene glycol) (PEG) or Glucose (GLC) derivatives; Functionalization of MNPs with cyclooctynylamine (CO) or dibenzocyclooctynylamine (DBCO) derivatives; Agarose gel electrophoresis and ζ-potential measurements of the different MNPs; MNP stability assays in water, DMEM (0 % FBS) and DMEM (10 % FBS); MNP reaction with N_3-PEG5000-NH_2 in suspension; Estimation of the number of CO and DBCO molecules per MNP using the fluorogenic click reaction with 3-azido-7-hydroxycoumarin; Fluorogenic click reaction with 3-azido-7-hydroxycoumarin in cell culture medium; Estimation of the number of MNPs attached to the substrate in the QCM experiments; XPS characterization of gold substrates functionalized with azide; Cell membrane labelling with DBCO-sulforhodamine B; Western Blot Ez-Blue Gel staining; Evaluation of cell morphology in cells treated with Ac_4ManNAz; Cell growth curves in the presence of Ac_4ManNAz; Time lapse of azide-modified glycoproteins labelled with DBCO-PEG_4-5/6-Sulforhodamine; MNP cytotoxicity assays; Fluorescence microscopy analysis of the click reaction of MNPs on cell membranes; Flow cytometry analysis of the MNPs click reactivity at different incubation times; TEM analysis of the MNP coupling with cells; Fluorescence spectra of the different types of MNPs.

AUTHOR INFORMATION

Corresponding Author

* Jesús M. de la Fuente (j.m.fuente@csic.es; jmfuente@unizar.es); Raluca M. Fratila (rfratila@unizar.es)

Author Contributions

J.I.L., J.M.F. and R.M.F. conceived and designed the study. J.I.L. conducted most of the experimental work, including the metabolic glycoengineering, the functionalization of the magnetic nanoparticles and the reactivity assessment in suspension, on surfaces and on cell membranes. E.M.A. synthesized the magnetic nanoparticles used throughout the study and performed their physicochemical characterization. M.E. carried out the synthesis of the cyclooctynylamine derivative **3**. All the authors analyzed and discussed the data. J.I.L. and R.M.F wrote the first draft of manuscript and all the authors contributed with critical revisions to the manuscript. J.M.A. obtained funding and supervised the experimental work of M.E. V.G., J.M.F. and R.M.F. obtained funding, supervised the experimental work of J.I.L. and E.M.A. and led the data analysis. All authors have given approval to the final version of the manuscript.

Funding Sources

This work has been supported by the European Commission, MagicCellGene Project (M-ERA.NET COFUND call 2016, funded by Ministerio de Economía y Competitividad, MINECO, Spain in the framework of the PCIN-2017-060 project), Ministerio de Innovación, Ciencia y Universidades (MCIU, PGC2018-096016-B-I00 to R.M.F), Ministerio de Economía, Industria y Competitividad (BIO 2017-84246-C2-1R to V. G. and J.M.F.) and MINECO and FSE/Agencia Estatal de Investigación (Ramón y Cajal subprogram, grant RYC-2015-17640 to R.M.F.). J.I.L. and E.M.A acknowledge financial support for their predoctoral fellowships from Gobierno de Aragón (DGA 2017-2021 call, co-funded by the Programa Operativo Fondo Social Europeo de Aragón 2014-2020) and Ministerio de Universidades (FPU17/02024), respectively. Authors also acknowledge support from Gobierno de Aragón and Fondos Feder for funding the Bionanosurf

(E15_20R) research group. J.M.A. and M.E. acknowledge support from the Basque Government (GIC-2015_IT-1033-16).

ACKNOWLEDGMENT

The authors would like to acknowledge the use of Servicios Científicos Técnicos del CIBA (IACS-Universidad de Zaragoza), the Advanced Microscopy Laboratory (Universidad de Zaragoza), for access to their instrumentation and expertise and the use of Servicio General de Apoyo a la Investigación-SAI, Universidad de Zaragoza. We also thank Pablo Martínez Vicente (Bionanosurf group, INMA, UNIZAR-CSIC) for help with the flow cytometry experiments and Silvia Ruiz-Rincón and Santiago Martín Solans (Platón group, UNIZAR) for assistance with the QCM experiments.

TOC Graphic

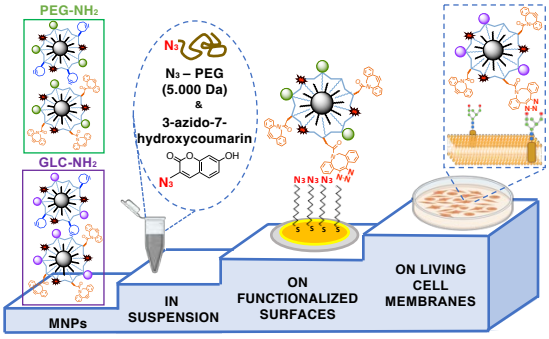

References

(1) Stephan, M. T.; Irvine, D. J. Enhancing Cell Therapies from the Outside in: Cell Surface Engineering Using Synthetic Nanomaterials. *Nano Today* **2011**, *6* (3), 309–325. https://doi.org/10.1016/j.nantod.2011.04.001.

(2) Lee, D. Y.; Cha, B.-H.; Jung, M.; Kim, A. S.; Bull, D. A.; Won, Y.-W. Cell Surface Engineering and Application in Cell Delivery to Heart Diseases. *Journal of Biological Engineering* **2018**, *12* (1), 28. https://doi.org/10.1186/s13036-018-0123-6.

(3) Tokunaga, T.; Namiki, S.; Yamada, K.; Imaishi, T.; Nonaka, H.; Hirose, K.; Sando, S. Cell Surface-Anchored Fluorescent Aptamer Sensor Enables Imaging of Chemical Transmitter Dynamics. *J Am Chem Soc* **2012**, *134* (23), 9561–9564. https://doi.org/10.1021/ja302551p.

(4) Jia, H.-R.; Zhu, Y.-X.; Duan, Q.-Y.; Wu, F.-G. Cell Surface-Localized Imaging and Sensing. *Chemical Society Reviews* **2021**, *50* (10), 6240–6277. https://doi.org/10.1039/D1CS00067E.

(5) He, Z.; Chen, Q.; Chen, F.; Zhang, J.; Li, H.; Lin, J.-M. DNA-Mediated Cell Surface Engineering for Multiplexed Glycan Profiling Using MALDI-TOF Mass Spectrometry. *Chemical Science* **2016**, *7* (8), 5448–5452. https://doi.org/10.1039/C6SC00215C.

(6) Damasceno, P. K. F.; de Santana, T. A.; Santos, G. C.; Orge, I. D.; Silva, D. N.; Albuquerque, J. F.; Golinelli, G.; Grisendi, G.; Pinelli, M.; Ribeiro dos Santos, R.; ~~Dominici, M.; Soares, M. B. P.~~ *et al.* Genetic Engineering as a Strategy to Improve the Therapeutic Efficacy of Mesenchymal Stem/Stromal Cells in Regenerative Medicine. *Frontiers in Cell and Developmental Biology* **2020**, *8*. https://doi.org/10.3389/fcell.2020.00737.

(7) Abbina, S.; Siren, E. M. J.; Moon, H.; Kizhakkedathu, J. N. Surface Engineering for Cell-Based Therapies: Techniques for Manipulating Mammalian Cell Surfaces. *ACS Biomaterials Science & Engineering* **2018**, *4* (11), 3658–3677. https://doi.org/10.1021/acsbiomaterials.7b00514.

(8) Custódio, C. A.; Mano, J. F. Cell Surface Engineering to Control Cellular Interactions. *ChemNanoMat* **2016**, *2* (5), 376–384. https://doi.org/10.1002/cnma.201600047.

(9) Yang, H. Surface Engineering of Macrophages with Nanoparticles to Generate a Cell-Nanoparticle Hybrid Vehicle for Hypoxia-Targeted Drug Delivery. *International Journal of Nanomedicine* **2009**, 25. https://doi.org/10.2147/IJN.S8339.

(10) Stephan, M. T.; Moon, J. J.; Um, S. H.; Bershteyn, A.; Irvine, D. J. Therapeutic Cell Engineering with Surface-Conjugated Synthetic Nanoparticles. *Nature Medicine* **2010**, *16* (9), 1035–1041. https://doi.org/10.1038/nm.2198.

(11) Lim, S.; Yoon, H. Y.; Jang, H. J.; Song, S.; Kim, W.; Park, J.; Lee, K. E.; Jeon, S.; Lee, S.; Lim, D.-K.~~; Kim, B.-S.; Kim, D.-E.; Kim, K.~~ *et al.* Dual-Modal Imaging-Guided Precise Tracking of Bioorthogonally Labeled Mesenchymal Stem Cells in Mouse Brain Stroke. *ACS Nano* **2019**, *13* (10), 10991–11007. https://doi.org/10.1021/acsnano.9b02173.

(12) Swiston, A. J.; Cheng, C.; Um, S. H.; Irvine, D. J.; Cohen, R. E.; Rubner, M. F. Surface Functionalization of Living Cells with Multilayer Patches. *Nano Letters* **2008**, *8* (12), 4446–4453. https://doi.org/10.1021/nl802404h.

(13) Farokhzad, O. C.; Karp, J. M.; Langer, R. Nanoparticle–Aptamer Bioconjugates for Cancer Targeting. *Expert Opinion on Drug Delivery* **2006**, *3* (3), 311–324. https://doi.org/10.1517/17425247.3.3.311.

(14) Thomsen, T.; Klok, H.-A. Chemical Cell Surface Modification and Analysis of Nanoparticle-Modified Living Cells. *ACS Applied Bio Materials* **2021**, *4* (3), 2293–2306. https://doi.org/10.1021/acsabm.0c01619.

(15) Kirpotin, D. B.; Drummond, D. C.; Shao, Y.; Shalaby, M. R.; Hong, K.; Nielsen, U. B.; Marks, J. D.; Benz, C. C.; Park, J. W. Antibody Targeting of Long-Circulating Lipidic Nanoparticles Does Not Increase Tumor Localization but Does Increase Internalization in Animal Models. *Cancer Research* **2006**, *66* (13), 6732–6740. https://doi.org/10.1158/0008-5472.CAN-05-4199.

(16) Algar, W. R.; Prasuhn, D. E.; Stewart, M. H.; Jennings, T. L.; Blanco-Canosa, J. B.; Dawson, P. E.; Medintz, I. L. The Controlled Display of Biomolecules on Nanoparticles: A Challenge Suited to Bioorthogonal Chemistry. *Bioconjugate Chemistry* **2011**, *22* (5), 825–858. https://doi.org/10.1021/bc200065z.

(17) Lamoot, A.; Uvyn, A.; Kasmi, S.; de Geest, B. G. Covalent Cell Surface Conjugation of Nanoparticles by a Combination of Metabolic Labeling and Click Chemistry. *Angewandte Chemie International Edition* **2021**, *60* (12), 6320–6325. https://doi.org/10.1002/anie.202015625.

(18) Idiago-López, J.; Moreno-Antolín, E.; de la Fuente, J. M.; Fratila, R. M. Nanoparticles and Bioorthogonal Chemistry Joining Forces for Improved Biomedical Applications. *Nanoscale Advances* **2021**, *3* (5), 1261–1292. https://doi.org/10.1039/D0NA00873G.

(19) Lim, S.; Kim, W.; Song, S.; Shim, M. K.; Yoon, H. Y.; Kim, B.-S.; Kwon, I. C.; Kim, K. Intracellular Uptake Mechanism of Bioorthogonally Conjugated Nanoparticles on Metabolically Engineered Mesenchymal Stem Cells. *Bioconjugate Chemistry* **2021**, *32* (1), 199–214. https://doi.org/10.1021/acs.bioconjchem.0c00640.

(20) Agard, N. J.; Prescher, J. A.; Bertozzi, C. R. A Strain-Promoted [3 + 2] Azide–Alkyne Cycloaddition for Covalent Modification of Biomolecules in Living Systems. *J Am Chem Soc* **2004**, *126* (46), 15046–15047. https://doi.org/10.1021/ja044996f.

(21) Yoon, H. Y.; Koo, H.; Kim, K.; Kwon, I. C. Molecular Imaging Based on Metabolic Glycoengineering and Bioorthogonal Click Chemistry. *Biomaterials* **2017**, *132*, 28–36. https://doi.org/10.1016/j.biomaterials.2017.04.003.

(22) Koo, H.; Lee, S.; Na, J. H.; Kim, S. H.; Hahn, S. K.; Choi, K.; Kwon, I. C.; Jeong, S. Y.; Kim, K. Bioorthogonal Copper-Free Click Chemistry in Vivo for Tumor-Targeted Delivery of Nanoparticles. *Angewandte Chemie - International Edition* **2012**, *51* (47), 11836–11840. https://doi.org/10.1002/anie.201206703.

(23) Shang, L.; Nienhaus, K.; Nienhaus, G. U. Engineered Nanoparticles Interacting with Cells: Size Matters. *Journal of Nanobiotechnology* **2014**, *12* (1), 5. https://doi.org/10.1186/1477-3155-12-5.

(24) Jiang, W.; Kim, B. Y. S.; Rutka, J. T.; Chan, W. C. W. Nanoparticle-Mediated Cellular Response Is Size-Dependent. *Nature Nanotechnology* **2008**, *3* (3), 145–150. https://doi.org/10.1038/nnano.2008.30.

(25) Mirshafiee, V.; Mahmoudi, M.; Lou, K.; Cheng, J.; Kraft, M. L. Protein Corona Significantly Reduces Active Targeting Yield. *Chemical Communications* **2013**, *49* (25), 2557. https://doi.org/10.1039/c3cc37307j.

(26) Fratila, R. M.; Navascuez, M.; Idiago-López, J.; Eceiza, M.; Miranda, J. I.; Aizpurua, J. M.; de la Fuente, J. M. Covalent Immobilisation of Magnetic Nanoparticles on Surfaces via Strain-Promoted Azide–Alkyne Click Chemistry. *New Journal of Chemistry* **2017**, *41* (19), 10835–10840. https://doi.org/10.1039/C7NJ01822C.

(27) Moros, M.; Hernáez, B.; Garet, E.; Dias, J. T.; Sáez, B.; Grazú, V.; González-Fernández, Á.; Alonso, C.; de la Fuente, J. M. Monosaccharides versus PEG-Functionalized NPs: Influence in the Cellular Uptake. *ACS Nano* **2012**, *6* (2), 1565–1577. https://doi.org/10.1021/nn204543c.

(28) Debets, M. F.; van Berkel, S. S.; Schoffelen, S.; Rutjes, F. P. J. T.; van Hest, J. C. M.; van Delft, F. L. Aza-Dibenzocyclooctynes for Fast and Efficient Enzyme PEGylation via Copper-Free (3+2) Cycloaddition. *Chem. Commun.* **2010**, *46* (1), 97–99. https://doi.org/10.1039/B917797C.

(29) Jewett, J. C.; Sletten, E. M.; Bertozzi, C. R. Rapid Cu-Free Click Chemistry with Readily Synthesized Biarylazacyclooctynones. *J Am Chem Soc* **2010**, *132* (11), 3688–3690. https://doi.org/10.1021/ja100014q.

(30) Moros, M.; Pelaz, B.; López-Larrubia, P.; García-Martin, M. L.; Grazú, V.; de la Fuente, J. M. Engineering Biofunctional Magnetic Nanoparticles for Biotechnological Applications. *Nanoscale* **2010**, *2* (9), 1746. https://doi.org/10.1039/c0nr00104j.

(31) Stepien, G.; Moros, M.; Pérez-Hernández, M.; Monge, M.; Gutiérrez, L.; Fratila, R. M.; las Heras, M. de; Menao Guillén, S.; Puente Lanzarote, J. J.; Solans, C.~~; Pardo, J.; de la Fuente, J. M.~~ *et al*. Effect of Surface Chemistry and Associated Protein Corona on the Long-Term Biodegradation of Iron Oxide Nanoparticles In Vivo. *ACS Applied Materials & Interfaces* **2018**, *10* (5), 4548–4560. https://doi.org/10.1021/acsami.7b18648.

(32) Varazo, K.; Droumaguet, C. le; Fullard, K.; Wang, Q. Metal Ion Detection Using a Fluorogenic 'Click' Reaction. *Tetrahedron Letters* **2009**, *50* (50), 7032–7034. https://doi.org/10.1016/j.tetlet.2009.09.166.

(33) Lim, H. J.; Saha, T.; Tey, B. T.; Tan, W. S.; Ooi, C. W. Quartz Crystal Microbalance-Based Biosensors as Rapid Diagnostic Devices for Infectious Diseases. *Biosensors and Bioelectronics* **2020**, *168*, 112513. https://doi.org/10.1016/j.bios.2020.112513.

(34) Pohanka, M. Overview of Piezoelectric Biosensors, Immunosensors and DNA Sensors and Their Applications. *Materials* **2018**, *11* (3), 448. https://doi.org/10.3390/ma11030448.

(35) Love, J. C.; Estroff, L. A.; Kriebel, J. K.; Nuzzo, R. G.; Whitesides, G. M. Self-Assembled Monolayers of Thiolates on Metals as a Form of Nanotechnology. *Chemical Reviews* **2005**, *105* (4), 1103–1170. https://doi.org/10.1021/cr0300789.

(36) Häkkinen, H. The Gold–Sulfur Interface at the Nanoscale. *Nature Chemistry* **2012**, *4* (6), 443–455. https://doi.org/10.1038/nchem.1352.

(37) Laughlin, S. T.; Bertozzi, C. R. Metabolic Labeling of Glycans with Azido Sugars and Subsequent Glycan-Profiling and Visualization via Staudinger Ligation. *Nature Protocols* **2007**, *2* (11), 2930–2944. https://doi.org/10.1038/nprot.2007.422.

(38) Du, J.; Meledeo, M. A.; Wang, Z.; Khanna, H. S.; Paruchuri, V. D. P.; Yarema, K. J. Metabolic Glycoengineering: Sialic Acid and Beyond. *Glycobiology* **2009**, *19*, 1382–1401. https://doi.org/10.1093/glycob/cwp115.

(39) Saxon, E.; Luchansky, S. J.; Hang, H. C.; Yu, C.; Lee, S. C.; Bertozzi, C. R. Investigating Cellular Metabolism of Synthetic Azidosugars with the Staudinger Ligation. *J Am Chem Soc* **2002**, *124* (50), 14893–14902. https://doi.org/10.1021/ja027748x.

(40) Chang, P. v.; Chen, X.; Smyrniotis, C.; Xenakis, A.; Hu, T.; Bertozzi, C. R.; Wu, P. Metabolic Labeling of Sialic Acids in Living Animals with Alkynyl Sugars. *Angewandte Chemie International Edition* **2009**, *48* (22), 4030–4033. https://doi.org/10.1002/anie.200806319.

(41) Han, S.-S.; Lee, D.-E.; Shim, H.-E.; Lee, S.; Jung, T.; Oh, J.-H.; Lee, H.-A.; Moon, S.-H.; Jeon, J.; Yoon, S.~~; Kim, K.; Kang, S. W.~~ *et al*. Physiological Effects of Ac4ManNAz and Optimization of Metabolic Labeling for Cell Tracking. *Theranostics* **2017**, *7* (5), 1164–1176. https://doi.org/10.7150/thno.17711.

(42) Han, S.-S.; Shim, H.-E.; Park, S.-J.; Kim, B.-C.; Lee, D.-E.; Chung, H.-M.; Moon, S.-H.; Kang, S.-W. Safety and Optimization of Metabolic Labeling of Endothelial Progenitor Cells for Tracking. *Scientific Reports* **2018**, *8* (1), 13212. https://doi.org/10.1038/s41598-018-31594-0.

(43) Baskin, J. M.; Prescher, J. A.; Laughlin, S. T.; Agard, N. J.; Chang, P. v.; Miller, I. A.; Lo, A.; Codelli, J. A.; Bertozzi, C. R. Copper-Free Click Chemistry for Dynamic in Vivo Imaging. *Proceedings of the National Academy of Sciences* **2007**, *104* (43), 16793–16797. https://doi.org/10.1073/pnas.0707090104.

(44) Jacquemet, G.; Carisey, A. F.; Hamidi, H.; Henriques, R.; Leterrier, C. The Cell Biologist's Guide to Super-Resolution Microscopy. *Journal of Cell Science* **2020**, *133* (11). https://doi.org/10.1242/jcs.240713.